INTERNATIONAL JOURNAL OF HYDROGEN ENERGY 42 (2017) 15679–15688

Available online at www.sciencedirect.com

ScienceDirect

journal homepage: www.elsevier.com/locate/he

Silver nanoparticle/r-graphene oxide deposited mesoporous-manganese oxide nanocomposite for pollutant removal and supercapacitor applications

Jothi Ramalingam Rajabathar [a,b,*], *Arun K. Shukla* [c], *Aldalbahi Ali* [a], *Hamad A. Al-Lohedan* [b]

[a] *Chemistry Department, College of Science, King Saud University, P.O. Box 2455, Riyadh 11451, Saudi Arabia*
[b] *Surfactant Research Chair, College of Science, King Saud University, P.O. Box 2455, Riyadh 11451, Saudi Arabia*
[c] *King Abdullah Institute for Nanotechnology, King Saud University, Riyadh 11451, Saudi Arabia*

ARTICLE INFO

Article history:
Received 4 January 2017
Received in revised form
11 March 2017
Accepted 6 April 2017
Available online 7 June 2017

Keywords:
Mesoporous MnO_2
Triton-100
Cr(VI) adsorption
Silver nanoparticles
Graphene oxide
Graphene

ABSTRACT

Mesoporous manganese oxide was prepared by a non-ionic surfactant route using Triton X-100, followed by Ag nanoparticle (NP) and graphene oxide incorporation by an ultrasonication-assisted process. Fine Ag NPs were incorporated into the tubular texture of mesoporous manganese oxide. The crystalline phase, particle size, and morphology of the prepared materials were characterized by X-ray diffraction (XRD), Barrett–Joyner–Halenda –Brunauer–Emmett–Teller analysis, scanning electron microscopy–energy dispersive X-ray analysis, and high-resolution transmission electron microscopy (HR-TEM). The XRD results confirmed the formation of the Mn_2O_3 phase for the as-prepared mesoporous manganese oxide and its nanocomposite. Very fine Ag NPs (<5–10 nm) were obtained. The mesoporous MnO_2 and graphene-incorporated Ag NPs/meso-MnO_2 had a tubular structure and "flaky pastry"-type morphology for the synthesized nanocomposites. HR-TEM images further confirmed the beautiful structural formation upon graphene addition and spherical/dot-shaped NP incorporation into the matrix of MnO_2. Improved surface area was obtained for the Ag NPs and graphene-incorporated mesoporous MnO_2 as compared to bulk MnO_2. The Cr(VI) removal analysis was performed using a batch technique, and enhanced removal of Cr(VI) was achieved (>98% removal of Cr(VI) within 1–2 h of reaction time) for Ag NP-incorporated mesoporous MnO_2. Efficient activity was observed because of the fine Ag NPs present in mesoporous manganese oxide, as opposed to the case of graphene oxide-doped meso-MnO_2 and pristine mesoporous meso-MnO_2.

Introduction

Porous and mesoporous MnO_2 are attractive compounds because of their low cost and non-toxic nature. MnO_2 plays an important role in removing heavy metal ions, degrading phenolic compounds, and oxidizing catalytic volatile organic compounds; further, it is a suitable candidate for battery and supercapacitor applications [1]. Ce-doped manganese oxide octahedral molecular sieve (OMS) materials and Ce–Mn oxide-based composites with the cryptomelane phase of manganese oxide show promising activity for the complete

* *Corresponding author*. Chemistry Department, College of Science, King Saud University, P.O. Box 2455, Riyadh 11451, Saudi Arabia. Fax: +966 1 4679972.
E-mail address: rjothiram@gmail.com (J.R. Rajabathar).
http://dx.doi.org/10.1016/j.ijhydene.2017.04.038
0360-3199/

oxidation of phenolic compounds by wet catalytic methods [2,3]. The surface area of ceria-based manganese oxides with porous tunnel-structured materials is five times higher than pristine MnO_2 [4]. Pang et al. reported a high specific capacitance (700 F g^{-1}) for MnO_2 materials in the form of thin films. Their finding sparked a huge interest in the energy storage device fabrication community for its application to super capacitor electrodes [5]. The advantages of silver nanoparticle are (a) simple feasible way of preparation, (b) low cost for mass production metal oxide nanocomposite, (c) effective antibacterial and catalytic oxidation property [5a–5c]. Hence, doping suitable silver nanoparticles (NPs) into the porous structure of MnO_2 could provide enhanced catalytic activity and alter the physicochemical properties. Nanda et al. reported mesoporous manganese oxide prepared by a cationic surfactant-assisted method and supported on MCM-41. They studied the complete structural characterization of different ratios of Mn/Si-incorporated meso-MnO_2/MCM-41 catalysts for photocatalytic dye degradation reactions [6a]. Graphene incorporation on mesoporous manganese oxide is further improves the electron mobility through carbon network and enhance its active surface area/sites in the surface structure [6b,6c]. Heavy metal ions cannot be degraded to harmless products, like organic pollutants, or biodegradable products [7]. Suitable methods for Cr(VI) removal from industrial wastewater and groundwater resources are being developed rapidly because of the toxic nature of this element. The common treatment methods include ion exchange [8,9], precipitation [10,11], membrane separation (such as ultrafiltration and reverse osmosis) [12,13], and electrochemical reduction of Cr(VI) [14]. However, most of these treatments have limitations, which include the generation of toxic sludge, high energy requirements, long treatment times, and poor removal efficiencies [15]. Recently, Zhan et al. used mesoporous silica KIT-6 as a template for the formation of meso-MnO_2 [16]. The adsorption of heavy metal ions, including Cr from aqueous solutions, is an effective and low cost removal technique [12]. The significant benefits of adsorption processes include effective and economical contaminant removal, recovery, and recycling of adsorbed metals from the adsorbent. Nanoparticle incorporation in the matrix of mesoporous metal oxide materials is of growing interest in the field of functional materials development and it could provide the enhanced catalytic and electro catalytic activity. To the best of knowledge, there is no report on non-ionic surfactant mediated synthesis of meso-MnO_2 followed by silver nanoparticle (Ag NPs) incorporation and graphene deposition to make nanocomposite catalyst fabrication. The detailed structural and morphology characterization has been studied. The prepared nanocomposite materials are further studied for hexavalent chromium sorption and supercapacitor performance for electrochemical energy storage application.

Experimental

Materials and methodology

All essential chemicals are obtained from Sigma Aldrich and used without further purification. Preparation of mesoporous MnO_2 is generally performed by co-precipitation, template assisted hydrothermal, micro emulsion methods. The XRD pattern of the powder sample is recorded using Miniflex 600. The morphology and particle size distribution of the nanoparticles were evaluated using Transmission electron microscopy (TEM; JEOL JEM-2100F) and dynamic light scattering (DLS; Brookhaven Instruments system). Branson digital sonifier®400 is used for ultra-sonication process. Surface area measurement and N_2-sorption isotherms were analyzed by NOVA 2200e model. The electrochemical experiments are carried out using three-electrode type cell. Briefly, the as-prepared material, acetylene black and nafion were mixed in a mass ratio of (80:10:10). Then it dispersed to produce a homogeneous paste. Then, prepared paste was coated onto the nickel foam to fabricate the working electrode. The silver/silver chloride electrode was utilized as the reference electrode and Platinum foil was used as the counter electrode. The all electrochemical analysis was carried out using CHI 600series electrochemical workstation.

Synthesis of meso-MnO_2 by non-ionic surfactant route

Mesoporous MnO_2 by a precipitation method using manganese sulfate ($MnSO_4$), Triton-X-100 as a non-ionic surfactant, ammonium persulfate ($NH_4S_2O_8$) as an oxidizing agent, and ammonia as a directing agent. Triton-100 (2 mL) was dissolved in a minimal amount of deionized water (240 mL) and stirred continuously for 60 min. Secondly, $MnSO_4$ (0.1 mol) was dissolved in a minimal amount of deionized water (50 mL). Then, ammonium persulfate (0.1 mol) was added to the $MnSO_4$ solution and stirred vigorously for 60 min at room temperature. After complete mixing, the ammonia solution (40 mL) was added and stirred vigorously for 90 min until precipitation was complete. The well-mixed surfactant was finally added into the prepared manganese (II) sulfate solution. The solution was continuously stirred for 12 h, and then filtered and dried at 120 °C to remove any volatile impurities. The resulting solid was calcined at 400 °C for 3 h for complete removal of the surfactant.

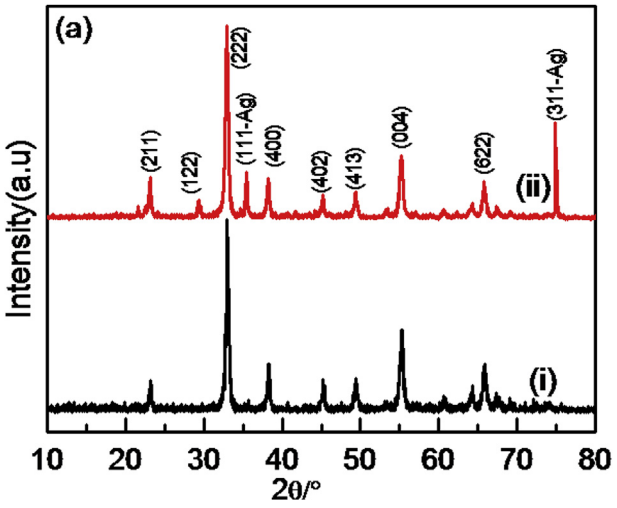

Fig. 1 – XRD pattern of (i) meso-MnO_2, (ii) AgNPs@meso-MnO_2 and Ag/Graphene–meso-MnO_2.

Table 1 – Crystallite size, surface area, pore size and elemental composition of (i) meso-MnO_2, (ii) AgNPs@meso-MnO_2, (iii) Graphene/AgNPs–meso-MnO_2.

No.	Sample name	Cyrstallite size (nm)	BET (m^2/g)	Pore volume (cc/g)	Pore size (nm)	Elemental composition (at%)			
						Mn	O	C	Ag
1	Mesoporous MnO_2	17.3	65	3.36×10^{-2}	1.1	22.56	45.90	31.54	–
2	AgNPs@Meso-MnO_2 nanocomposite	14.4	55	2.93×10^{-2}	1.4	21.29	45.78	32.54	0.39
3	AgNPs@Meso-MnO_2 nanocomposite	14.2	54	2.91×10^{-2}	1.3	10.39	35.94	53.61	0.06

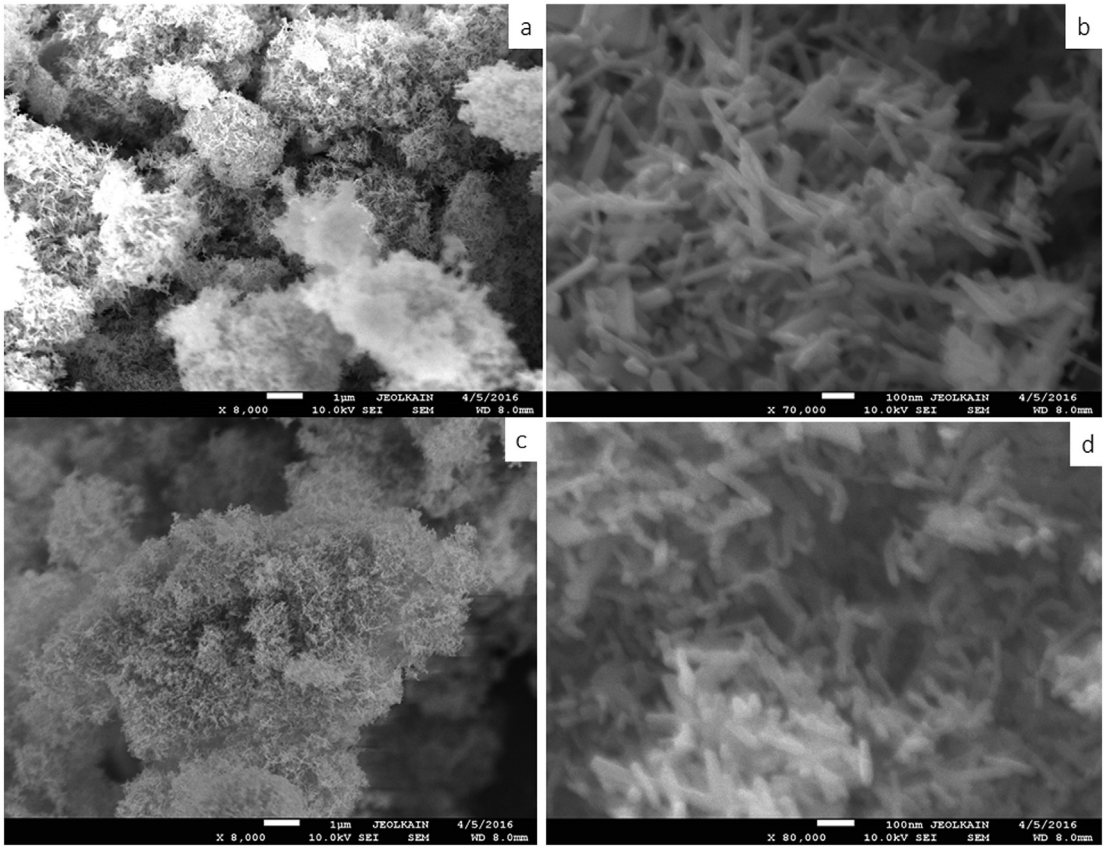

Fig. 2 – (a–b) SEM images of AgNPs@meso-MnO_2 (c–d) SEM images of after chromium adsorption on AgNPs@meso-MnO_2.

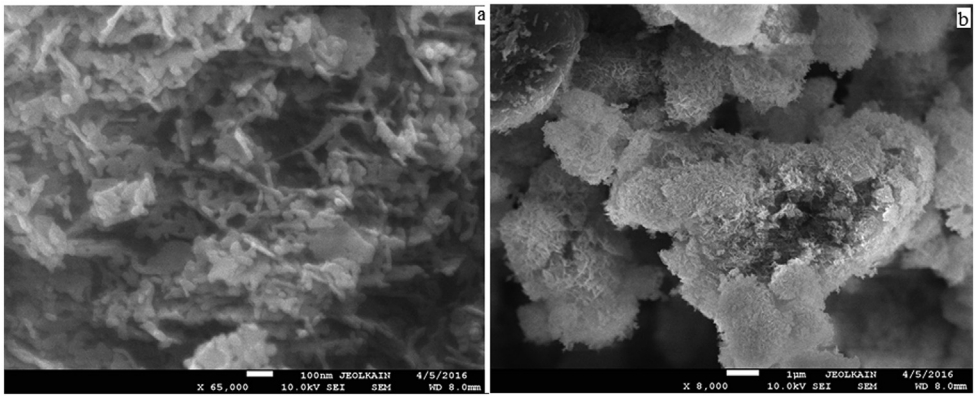

Fig. 3 – (a–b) SEM images of Graphene/AgNPs–meso-MnO_2.

Synthesis of AgNPs@meso-MnO_2 and graphene–AgNPs/meso-MnO_2

Silver nanoparticle doping is carried out by ultra-sonication process. The appropriate amount of silver nitrate is dissolved in ethanol solution and ultra-sonicated for 10 min at 20% amplitude of power. After 10 min, 1 g of as prepared meso-MnO_2 is added into the silver nanoparticle solution (0.001 g of $AgNO_3$ added in 10 mL of ethanol solution and ultra-sonicated for 10 min with amplitude power of 20%) and continues to ultrasonicate further 10 min followed by dried at 80 °C. The prepared silver nanoparticle doped mesoporous MnO_2 is designated as AgNPs@meso-MnO_2. The silver nanoparticle graphene deposited meso-MnO_2 nanocomposite was prepared the same way AgNPs@meso-MnO_2, the only difference is to addition of graphene oxide. The appropriate amount of graphene oxide powder (0.01 g) was mixed together with Ag NPs and dispersed meso-MnO_2 in ethanol solution. The dispersed solid solution is further ultra-sonicated at 20% amplitude power of ultra-sonication for 20 min. The ultra-sonicated graphene–silver nanoparticle mixed meso-MnO_2 was dried at 80 °C. The as prepared material is designated as Graphene/AgNPs@meso-MnO_2. The as prepared all catalyst including pristine meso-MnO_2 is tested for the analysis of chromium (VI) removal process. Branson digital sonifier®400 is used for ultra-sonication process.

Hexavalent Cr(VI) adsorption experiment

The adsorption tests were carried out to investigate the chromium adsorption efficiency of the nanomaterial. In the experiments, the Cr(VI) solution with desired concentration was prepared by dissolving potassium chromate in 18 MΩ of milli-Q water (Millipore, USA) with pH 6 ± 0.2. The 100 mg of each of adsorbent nanomaterial samples were added into separate glass bottle containing 15 mL of Cr(VI) solution with 50 mg/L concentration at room temperature and stirred 200 rpm using a shaker for 24 h. The solution samples were excluded at defined 1 h time interval during adsorption for the analysis of Cr(VI) concentration in the solution. The solutions were filtered by 2 μm filter and determined the concentration by Atomic Adsorption Spectrometer (AAS) from Agilent Technologies 200 series AA. The above adsorption processes were performed in triplicate under same condition and adsorption percentage was calculated by the following equation:

$$\text{Cr(VI) adsorption (\%)} = \left(1 - \frac{C_f}{C_i}\right) \times 100$$

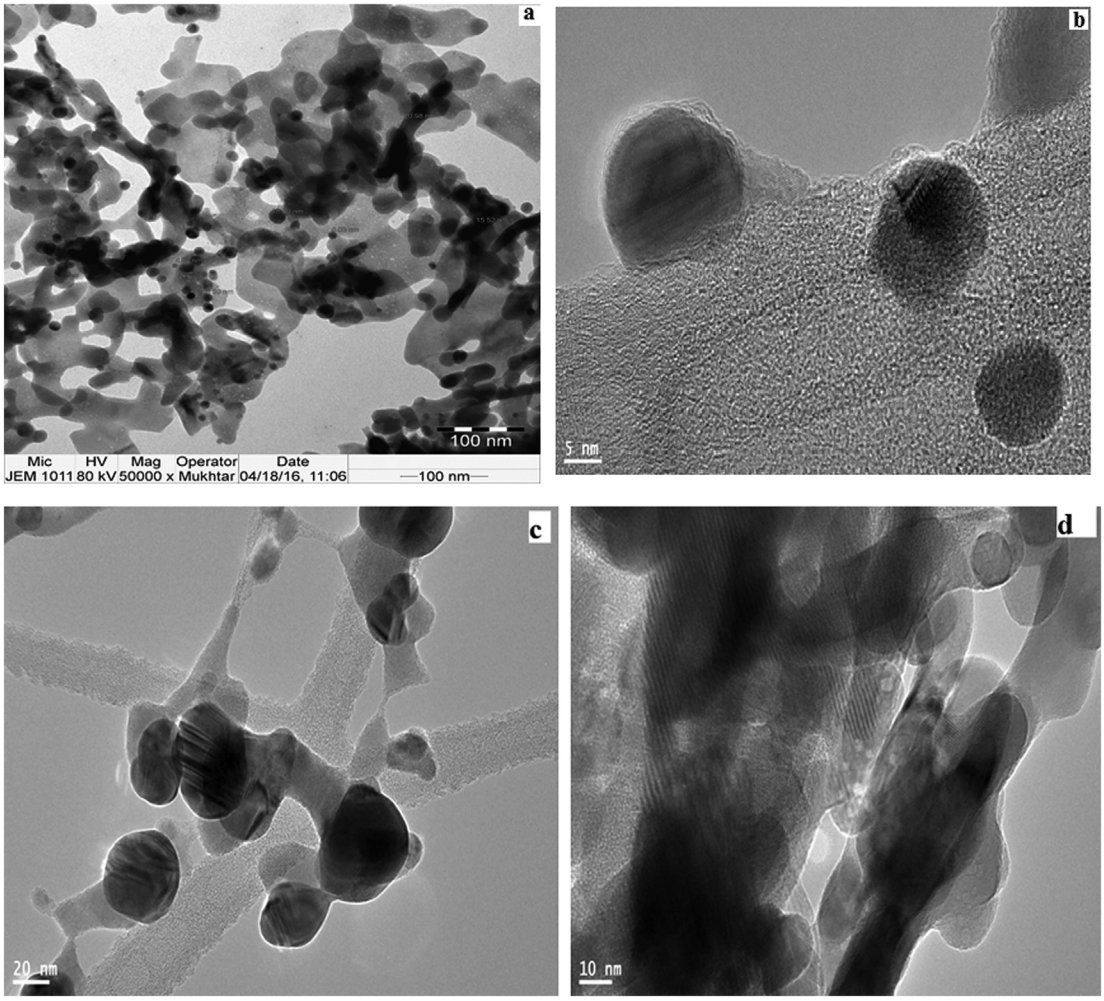

Fig. 4 – (a–d) HR-TEM images of AgNPs@meso-MnO_2.

where C_i initial concentration of chromium, C_f final concentration of chromium.

Results and discussion

The X-ray diffraction pattern of mesoporous MnO_2 prepared using the non-ionic surfactant (Triton X-100) is shown in Fig. 1(a). The Ag NP-incorporated mesoporous MnO_2 is shown in Fig. 1(b). The major intense peaks are indexed and referred with standard powder diffraction data. The as-prepared mesoporous MnO_2 corresponded well to JCPDS file number 24-0508 for the Mn_2O_3 phase of manganese oxide; the d-spacing values and crystalline *hkl* values are similar to the reported literature values for meso-MnO_2 prepared by other methods [15]. The average crystallite size of the prepared meso-MnO_2 nanocomposite material was calculated using the Scherer equation; the results are listed in Table 1. Similar X-ray diffraction patterns and Mn_2O_3 phases were obtained for both the Ag NPs and graphene-incorporated mesoporous manganese oxide nanocomposite. The morphology and textural property variations are shown in the clear images, and the difference between the Ag NPs/meso-MnO_2 and graphene-Ag NP deposited meso-MnO_2 nanocomposite was analyzed using SEM, high-resolution TEM (HR-TEM), and Brunauer–Emmett–Teller (BET) analysis. The elemental compositions of AgNPs@meso-MnO_2, graphene/AgNPs@meso-MnO_2, and meso-MnO_2 are also shown in Table 1. The presence of atomic percentages of the respective elementals in the prepared samples is discussed below, and the respective energy dispersive X-ray (EDX) maps are shown as separate images. Fig. 2(a–b) contains SEM images of AgNPs@meso-MnO_2 (8000× and 70,000× magnifications) that show the fibrous nanotube morphology for Ag@meso-MnO_2. Fig. 2(a) shows an SEM image (8000× magnification) of the spherical shape nucleation of nanotubes formation occurs and agglomerated spherical shapes at higher magnification. Fig. 2(b) clearly shows the formation of tubular shapes for Ag@meso-MnO_2. Fig. 2(c–d) shows SEM images of Ag@meso-MnO_2 after Cr sorption onto the surface of meso-MnO_2. Cr(VI) absorption onto the mesoporous manganese oxide surface appears to have a fibrous and agglomerated spherical morphology. The SEM images in Fig. 2(c–d) clearly indicate that the morphology of the nanocomposite is predominantly unaffected after Cr adsorption. The nanocomposite retained the same shape after the adsorption process.

Fig. 3 shows SEM images of the graphene/AgNPs@meso-MnO_2 nanocomposite; the flaky structure of the graphene sheets is visible in Fig. 3(a–b). Similarly, a tubular morphology was obtained for the meso-MnO_2 with flaky graphene deposition on the surface. Fig. 3(b) shows the aggregated particle formation for the tubular morphology of the prepared nanocomposite at a higher magnification.

Fig. 4(a–d) shows images of Ag NP formation and dispersion on the tubular mesoporous MnO_2. Fig. 4(a) shows the small tubular shape of the MnO_2 nanotubes together with the black particles that indicate Ag NP deposition on the surface of the manganese oxide lattice. The dark color of the particles is due to the metal-rich characteristic of the Ag NP deposition.

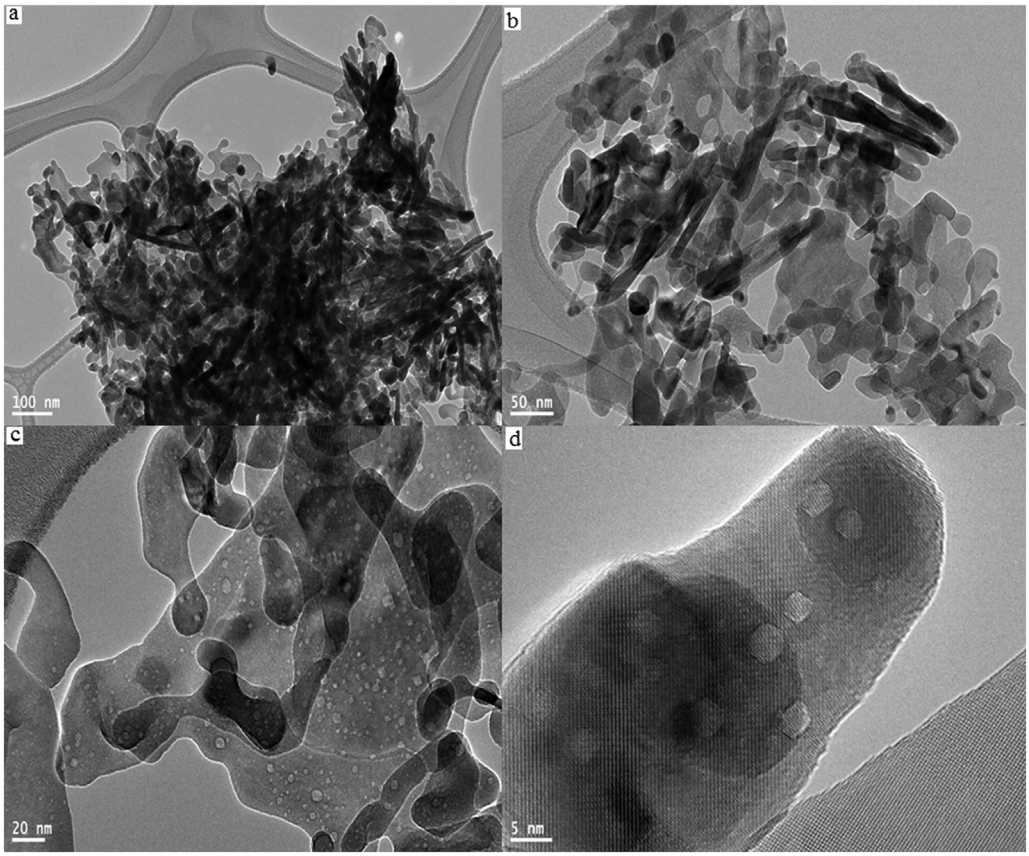

Fig. 5 – (a–d) HR-TEM images of Graphene/AgNPs–meso-MnO_2.

The diameter of each Ag NP is measured from the TEM image (Fig. 4(a), red lines). The Ag NPs were 5–15 nm on the porous structure of MnO_2. Fig. 4(b) shows the formation of very fine individual Ag NPs on the mesoporous manganese oxide surface because of the ultra-sonication-assisted process, which is quite visible at a 5-nm scale in the HR-TEM images (e.g., spherical and square-type Ag NPs were obtained). Fig. 4(c) shows the darker spherical particles that formed because of the metal-rich particle aggregation. Fig. 4(d) shows the fine square shape of the NP incorporation/deposition into the manganese oxide nanotube structures (Fig. 4(b) and (d)).

Fig. 5(a–d) shows the HR-TEM images of the graphene/AgNPs–meso-MnO_2 nanocomposite prepared by the ultra-sonication-assisted deposition process. Fig. 5(a) shows the strong deposition and incorporation of Ag NPs on the tubular morphology of the mesoporous manganese oxide together with the graphene sheets. Fig. 5(b) shows the flaky graphene sheets dispersed on the mesoporous MnO_2 together with the spherical dot shapes of the Ag NPs. Fig. 5(c–d) shows higher magnification micrographs, which are equivalent to the nanometer scale in the 5–20 nm range. Very fine Ag NPs (white dots and square-shaped particles) formed on the sheets of the graphene/meso-MnO_2 nanocomposite. Fig. 5(d) shows the fine spherical and square particles that formed with sizes <5 nm for the graphene/AgNPs–meso-MnO_2 nanocomposite.

The N_2 sorption-desorption behavior of the mesoporous MnO_2 and its composite form have been studied by BET and Barrett–Joyner–Halenda (BJH) analysis, and the active surface area of the mesoporous MnO_2, Ag NP-incorporated meso-MnO_2 and graphene/Ag NP incorporated meso-MnO_2 are shown in Fig. 6(a–c) and Table 1. The isotherms for the Ag NPs deposited on meso-MnO_2 and the parent samples (meso-MnO_2) display the type IV isotherm with a H3 hysteresis loop that mostly agrees with the presence of aggregated tubular nanofiber-like particles [17]. The BJH pore size distribution of the meso-MnO_2 samples specifies the mesoporous nature with sizes of 2–15 nm. The BET surface area and corresponding pore radius of meso-MnO_2, Ag@meso-MnO_2, and graphene/Ag@meso-MnO_2 are 65, 55, and 54 $m^2\ g^{-1}$ and 1.1, 1.4, and 1.3 nm, respectively (Table 1). The graphene and Ag NP/meso-MnO_2 NPs with a precise surface area (55 & 54 $m^2\ g^{-1}$) and pore radius (1.4 & 1.3 nm) is prominent for the metal sorption studies as it offers a higher active surface area for the sorption reactions. SEM–EDX elemental content mapping of the AgNPs@meso-MnO_2 and graphene/AgNPs@meso-MnO_2 are shown in Fig. 7(a–b). The elemental content in the Ag NP-incorporated meso-MnO_2 and graphene/

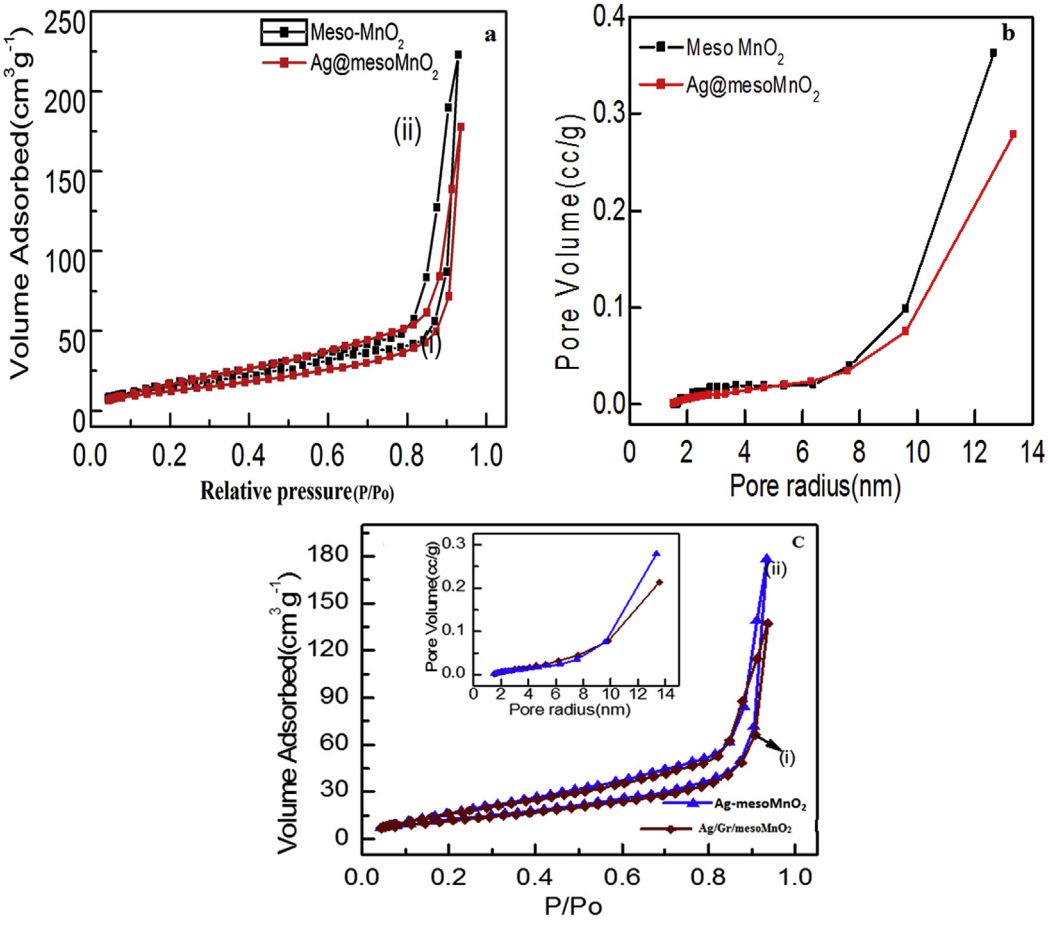

Fig. 6 – (a) N_2 – adsorption–desorption and (b) BJH pore size measurements meso-MnO_2 (blue) and AgNPs–meso-MnO_2 (red), (c) comparative pore size distribution of AgNPs–meso-MnO_2 (blue) and Graphene/AgNPs–meso-MnO_2 (blue). (For interpretation of the references to color in this figure legend, the reader is referred to the web version of this article.)

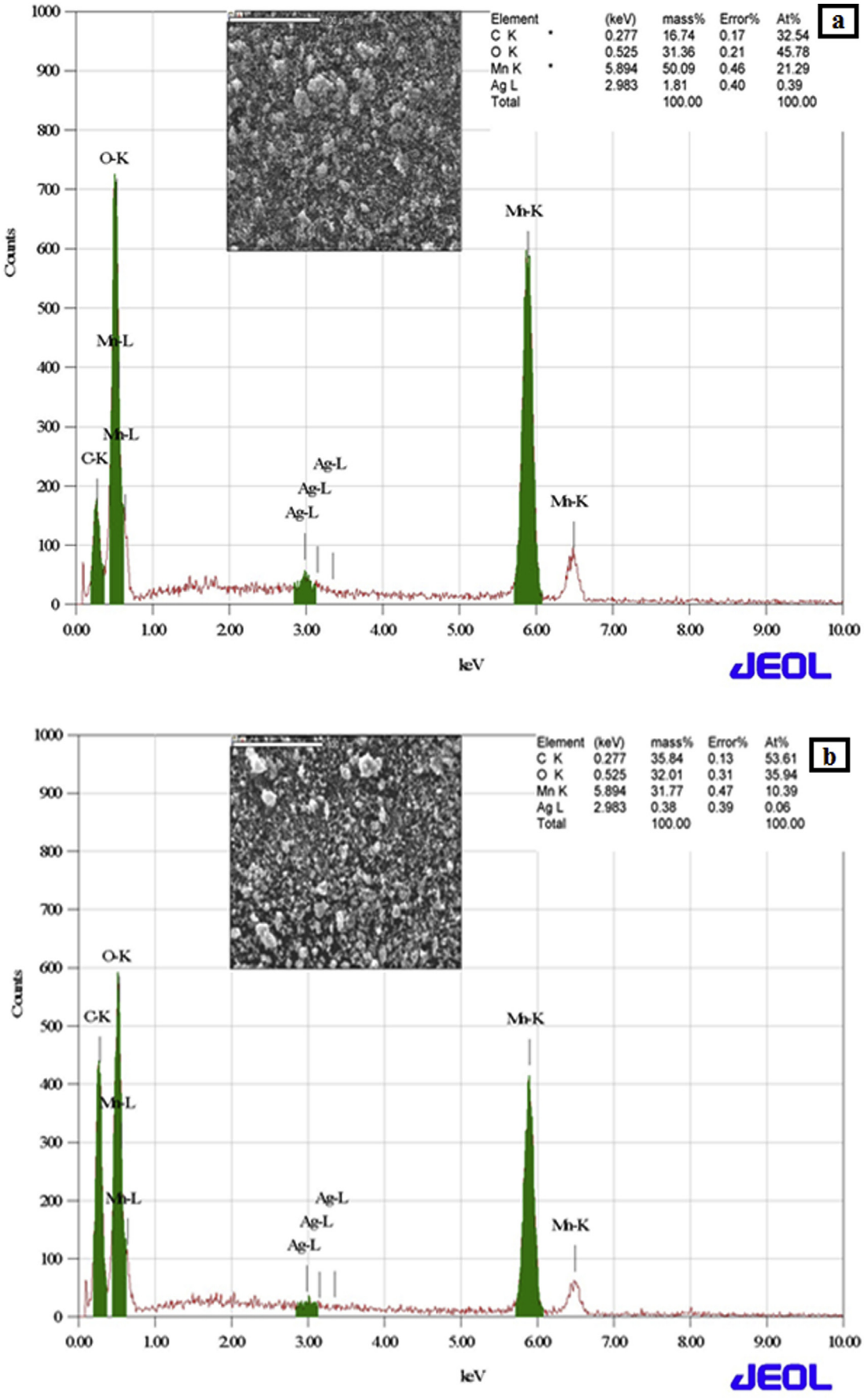

Fig. 7 – SEM–EDX analysis of (a) AgNPs@meso-MnO_2 (b) Graphene/AgNPs–meso-MnO_2.

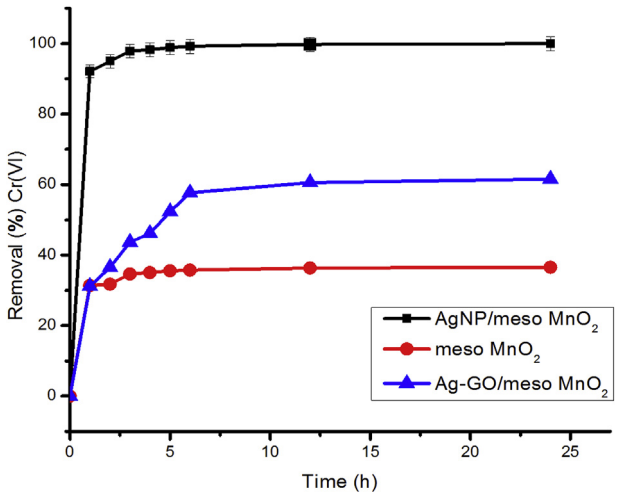

Fig. 8 – Hexavalent chromium removal efficiency on pristine meso-MnO_2 (red), AgNPs/meso-MnO_2 (black) and Graphene/AgNPs–meso-MnO_2 (blue) nanocomposite catalysts. (For interpretation of the references to color in this figure legend, the reader is referred to the web version of this article.)

AgNP-incorporated meso-MnO_2 is clearly distinguished by the SEM–EDX analysis. Double the atomic amount (%) of the expected carbon content was observed for graphene/AgNPs–meso-MnO_2 samples (Fig. 7(b)). At the same time, a decrease of the Ag NP content was observed after graphene deposition on mesoporous MnO_2 because of the charge adjustment in the MnO_2 lattice. The source of the polymeric carbon was from graphene oxide and the partial decomposition of the surfactant molecules.

Fig. 8(a–c) shows the application of the as-prepared mesoporous MnO_2, Ag NP-incorporated meso-MnO_2 and graphene/Ag-NPs-incorporated meso-MnO_2 for the removal of toxic Cr(VI) from the aqueous medium. The Ag NP incorporation onto meso-MnO_2 provided an excellent sorption capacity for Cr(VI) adsorption compared to graphene/AgNPs–meso-MnO_2 and pristine meso-MnO_2. The Cr(VI) removal capacities obtained for graphene/AgNPs–meso-MnO_2 and AgNPs–meso-MnO_2 are 68% and 98%, respectively (Table 2). The calculated adsorption capacities were approximately 460 mg/g and 140 mg/g for AgNPs/meso-MnO_2 and graphene/AgNPs/meso-MnO_2. The main reason for the increased sorption activity is the presence of Ag NPs and MnO_2–polymeric carbon in the meso-MnO_2 nanocomposite. Hence, the fine Ag NPs that were deposited on the mesoporous MnO_2 matrix could provide an increased affinity for Cr(VI) sorption (Fig. 8(a)). The porous nature of MnO_2 and the fine Ag NPs act as effective catalytic sites for the enhanced adsorption process on the manganese oxide surface.

The comparative hexavalent chromium sorption activity and capacity on different route prepared porous manganese oxide composite are shown in Table 2. The higher concentration (50 mg/L) of hexavalent chromium is tested on present method prepared Ag NPs/meso-MnO_2 compared to other recent reports, which normally tested using 10 mg/L concentration of phenol solution. Most of recent research related with nanocomposite catalyst for hexavalent chromium removal analysis studied with low concentration of chromium (VI) precursor [18–27]. Graphene deposition in manganese oxide not favors higher absorption capacity for chromium due to hydrophobic nature of carbon network. It shows average activity and only silver nanoparticle incorporated meso-MnO_2 shows higher absorption capacity due to mesoporous nature of the prepared catalyst.

Du et al (2014) reported, Cr(VI) removal efficiency (96.0–99.98%) at initial Cr(VI) concentration of 10 mg/L and pH 2.0 or (8.0) was observed over the MnO_2-coated diatomite samples with different morphologies, and the maximal Cr(VI) adsorption capacity reached 101 mg/g over the wire-like MnO_2/diatomite catalyst. In the present method prepared Ag NPs incorporated meso-MnO_2 and graphene deposited catalyst are showing good recyclability showing after washing the used catalyst followed by dried in hot air oven at 80–90 °C. Two possible ways of mechanism are used to explain the hexavalent chromium adsorption on metal oxide catalyst such as the ion-exchange and electrostatic attraction of hexavalent chromium on the surface of metal oxide [28]. In the present work, as prepared catalysts do not contain any interlayer cation due to its mesoporous form and hence the possible mechanism related with chromium sorption was purely an electrostatic interaction. The higher efficiency and quick removal chromium in aqueous medium by AgNPs/meso-MnO_2 and graphene deposited meso-MnO_2 nanocomposite are promising catalytic materials for heavy metal removal study. The newly prepared materials are tested for electrochemical supercapacitor analysis. Fig. 9 shows the charge and discharge cycling performance of the graphene deposited MnO_2 nanocomposite electrode. The specific capacitance of the same is calculated based typical capacitance equation. The obtained capacitance of 150.3 F/g at the scan rate of 0.001 V/s and its showing enhanced supercapacitance value compared to other route prepared manganese oxide nanocomposite electrode [29]. In future, the prepared materials are planning to study in detail to enhance the super capacitance values.

Table 2 – The comparative activity of Ag/Graphene/meso-MnO_2 nanocomposite with reported catalyst.

Sorbent	Concentration of reactant (Cr(VI))	Removal rate	Adsorbed amount (mg/g)	Ref
MnO_2 modified expanded graphite	2 mg/L	90%	3.0	[21]
MnO_2 deposited diatomite	10 mg/L	96%	61.0	[19]
AgNPs/meso-MnO_2	50 mg/L	98%	460	Present work
Graphene/AgNPs/meso-MnO_2	50 mg/L	68%	140	Present work

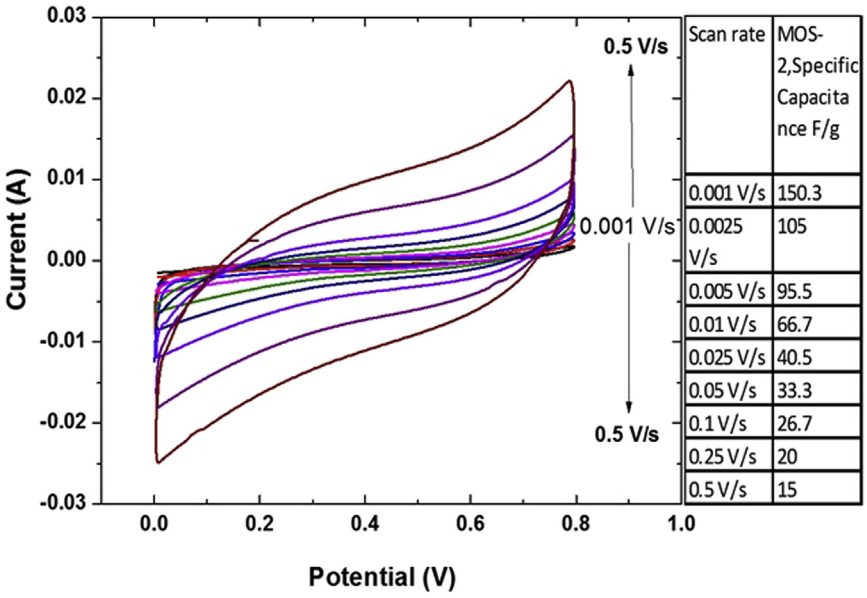

Scan rate	MOS-2,Specific Capacitance F/g
0.001 V/s	150.3
0.0025 V/s	105
0.005 V/s	95.5
0.01 V/s	66.7
0.025 V/s	40.5
0.05 V/s	33.3
0.1 V/s	26.7
0.25 V/s	20
0.5 V/s	15

Fig. 9 – Electrochemical activity and supercapacitance performance of Graphene/meso-MnO_2 nanocomposite.

Conclusions

Mesoporous manganese oxide is successfully prepared by direct one step process using Triton-X100 surfactant assistance followed by fabrication of Ag@meso-MnO_2 and Graphene/AgNPs–meso-MnO_2 nanocomposites *via* faster ultrasonication process. X-ray diffraction patterns confirm the Mn_2O_3 phase formation for both silver and graphene deposited meso-MnO_2. HR-TEM images confirm the tubular nanostructure for manganese oxide and spherical and square type of silver nanoparticle below 5–10 nm are dispersed on MnO_2 support. Flaky morphology observed for graphene formation on mesoporous manganese oxide. The TEM images are clearly showing the exact formation find nanoparticle and graphene formation on MnO_2 matrix. SEM–EDX and BET analysis are showing elemental content present in the nanocomposite with improved surface area values for silver and graphene dispersed meso-MnO_2 compared bulk MnO_2. The prepared nanocomposite are showing very good activity (>98%) for Ag NPs/meso-MnO_2 towards adsorption activity (460 mg/g) of Chromium (VI) in aqueous medium. Very fine silver nanoparticle deposition on the tubular nanostructure morphology of mesoporous manganese oxide could be the main cause for enhanced activity for hexavalent chromium removal. Both silver and graphene incorporated mesoporous MnO_2 nanocomposite could also act as promising electro catalyst for super capacitor energy storage applications.

Acknowledgment

The authors are grateful to Deanship of Scientific Research; the authors (HAA) also thank the research chair. This project was supported by King Saud University, Deanship of Scientific Research, College of Science-Research Center.

REFERENCES

[1] Suib SL. Acc Chem Res 2008;41:479–87.
[2] Jothiramalingam R, Wang MK. J Hazard Mater 2007;147:562–9.
[3] Abecassis-Wolfovich M, Jothiramalingam R, Landau MV, Herskowitz M, Viswanathan B, Varadarajan TK. Appl Catal B Environ 2005;59:91–8.
[4] Jothiramalingam R, Viswanathan B, Varadarajan TK. Catal Commun 2005;6:41–5.
[5] (a)Pang SC, Anderson MA, Chapman TW. J Electrochem Soc 2000;147:444–50.
(b)Altın I, Sökmen M. Water Air Soil Pollut 2014;225:1786–8.
(c)Kunkalekar RK, Prabhu MS, Naik MM, Salker AV. Colloids Surf B Biointerfaces 2014;113:429–34.
[6] (a)Nanda B, Pradhan AC, Parida KM. Microporous Mesoporous Mater 2016;226:229–42.
(b)Wan Shunli, He Feng, Wu Jiayu, Wan Wubo, Gu Yawei, Gao Bin. J Hazard Mater 2016;314:32–40.
(c)Naderi HR, Norouzi P, Ganjali MR. Appl Surf Sci 2016;366:552–60.
[7] Khezami L, Capart R. J Hazard Mater 2005;123:223–31.
[8] Rengaraj S, Yeon KH, Moon SH. J Hazard Mater 2001;87:273–87.
[9] Rivero MJ, Primo O, Ortiz MI. J Chem Technol Biotechnol 2004;79:822–9.
[10] Kurniawan TA, Chan GYS, Lo W, Ba-bel S. Chem Eng J 2006;118:83–98.
[11] Mohan D, Rajput S, Singh VK, Steele PH, Pittman CU. J Hazard Mater 2011;188:319–33.
[12] Barakata MA, Schmidt E. Desalination 2010;256:90–3.
[13] Kozlowski CA, Walkowiak W. Water Res 2002;36(19):4870–6.
[14] Martinez SA, Rodriguez MG. J Chem Technol Biotechnol 2007;82:582–7.

[15] Mittal A, Krishnan L, Gupta VK. Sep Purif Technol 2005;43:125–33.
[16] Zhan S, Zhu D, Qiu M, Yu H, Li Y. RSC Adv 2015;5:29353–61.
[17] Said S, Riad M, Helmy M, Mikhail S, Khalil L. Chem Mater Res 2014;6:27–41.
[18] Du Y, Zheng G, Wang J, Wang L, Wu J, Dai H. Microporous Mesoporous Mater 2014;200:27–34.
[19] Du Y, Wang L, Wang J, Zheng G, Wu J, Dai H. J Environ Sci 2015;29:71–81.
[20] Gheju M, Balcu I, Vancea C. J Environ Manag 2016;170:145–51.
[21] Jin H, Yuan J, Hao H, Ji Z, Liu M, Hou S. Mater Lett 2013;110:69–72.
[22] Bagheri M, Younesi H, Hajati S, Borghei SM. Int J Biol Macromol 2015;80:431–44.
[23] Madhu Kumari, Pittman Jr Charles U, Mohan D. J Colloid Interface Sci 2015;442:120–32.
[24] Dima JB, Sequeiros C, Zaritzky NE. Chemosphere 2015;141:100–11.
[25] Ma L, Xi Y, He H, Ayoko GA, Zhu R, Zhu J. Appl Clay Sci 2016;120:9–15.
[26] Jin H, Yuan J, Hao H, Ji Z, Liu M, Hou S. Mater Lett 2013;110:69–72.
[27] Hyder AHMG, Begum Shamim A, Egiebor Nosa O. J Environ Chem Eng 2015;3:1329–36.
[28] Hu J, Chen G, Lo IMC. Water Res 2005;39:4528–36.
[29] Li S, Qi L, Lu L, Wang H. Cotton-assisted preparation of mesoporous manganese oxide for supercapacitors. RSC Adv 2012;2:6741–3.